Probing the dynamics of instability in zeolitic materials

2004 J. Phys.: Condens. Matter 16 S3459

(http://iopscience.iop.org/0953-8984/16/33/006)

INSTITUTE OF PHYSICS PUBLISHING JOURNAL OF PHYSICS: CONDENSED MATTER

J. Phys.: Condens. Matter **16** (2004) S3459–S3472 PII: S0953-8984(04)79892-6

Probing the dynamics of instability in zeolitic materials

Neville Greaves[1] **and Florian Meneau**[1,2]

[1] Institute of Mathematical and Physical Sciences, University of Wales, Aberystwyth SY23 3BZ, UK
[2] Royal Institution of Great Britain, 21 Albemarle Street, London W1X 4BS, UK

E-mail: gng@aber.ac.uk (Neville Greaves)

Received 22 April 2004
Published 6 August 2004
Online at stacks.iop.org/JPhysCM/16/S3459
doi:10.1088/0953-8984/16/33/006

Abstract

Zeolites collapse under modest pressure or temperature, their microporous structures transforming into glasses of conventional density. Using *in situ* synchrotron radiation diffraction methods we show how pressure and temperature-induced amorphization are equivalent processes and that these are mirrored by changes in the local structure of charge compensating cations. Evidence for a low density amorphous phase and a high density amorphous phase present during zeolite collapse emerges from small angle scattering experiments. Combining powder diffraction with increasing temperature or pressure, we find that the thermobaric characteristics for zeolite collapse have negative $\mathrm{d}T/\mathrm{d}P$ slopes, consistent with increasing density during amorphization. However, this is not confined to a single melting curve but, instead, the regime extends over a significant region of T–P space. Moreover, zeolite amorphization involves depressurization and cavitation effects which can be used to set empirical boundaries for the stability of the low density amorphous phase. Within the region of zeolite instability the pressure or temperature of amorphization is found to be governed by the rate at which the stress is introduced—the more rapid this is, the higher the pressure or temperature the zeolite structure survives to. The temperature dependence of the rate of collapse is Arrhenian, suggesting that the initial low density amorphous phase has the characteristics of a superstrong liquid in contrast to the fragility of a conventionally melt quenched glass. Possibilities for creating 'perfect glasses' from the collapse of microporous crystals are discussed.

(Some figures in this article are in colour only in the electronic version)

1. Introduction

When glasses are formed conventionally from the melt, the dynamics of crystallization are bypassed and instead the configurations and free volume of the liquid state become frozen

into a highly entropic disordered structure. The amorphous state can also be reached directly from the crystalline solid state by the application of pressure [1]. Crystalline structures may also be destabilized to form amorphous structures by ion implantation [2], or by the use of shock waves [3] or grinding [4]. Sometimes transformation to the amorphous state can be achieved thermally at temperatures well below the meting temperature, T_m [5]. All of these low temperature solid state melting processes are generally referred to as 'amorphization' [6] and often result from compression [1] but sometimes decompression [5, 7].

Considering the Clausius–Clapeyron relation, $dT/dP = \Delta V/\Delta S$, where ΔV and ΔS are the volume and entropy of fusion, compressive amorphization should equate with a negative melting curve ($dT/dP < 0$) and decompressive amorphization with the more usual positive melting curve ($dT/dP > 0$). In general both types of melting curve should occur for a given phase, subtending a melting temperature maximum at some pressure. In the case of silica and its crystalline polymorphs, melting maxima occur at positive pressures [6], but for hexagonal ice, many silicate and aluminosilicate minerals [8] and also diamond silicon [9], melting maxima are predicted at negative pressures—a region which is generally empirically inaccessible, except by simulation. Negative pressure melting maxima though can be inferred experimentally when $dT/dP < 0$ occurs as the pressure is increased from ambient. $\Delta V < 0$ and $\Delta S > 0$ are the conditions necessary for compressive amorphization [6]. Interestingly, where different crystalline phases exist with the same composition but different density, dT/dP can take very different values over the same range of temperatures and pressure [6]. In particular in the few cases where microporous phases have been studied, like silicon clathrates [9] and porous silicon [10], melting temperatures are depressed and melting curves have steeper negative slopes compared to polymorphs of conventional density.

Experimentally, amorphization is generally either pressure-induced or temperature-induced—not both, as one is usually compressive and the other decompressive. For zeolites, though, we have shown that compressive amorphization can be triggered not just by pressures of a few gigapascals but also by temperatures close to the glass transition temperature, T_g [11–13]. In the case of temperature-induced amorphization we draw attention to the fact that for melt quenched glasses T_g is a fraction of the melting temperature, T_g/T_m being typically $\sim$0.6. Accordingly amorphization occurs at viscosities equivalent to 10^{12} Pa s or greater compared to values of around 10^2 Pa s operating at T_m. 10^{12} Pa s is the viscosity where the structural relaxation time is of the order of one or two minutes and where flow is imperceptible on experimental timescales and a rigid glass prevails [14].

In the first part of this paper we review how synchrotron radiation *in situ* x-ray techniques can be used to determine dT/dP, as well as the stability limits in $T-P$ space of the zeolite and the final glass. By considering anomalous behaviour in the thermal expansion coefficient, α, of the zeolite during thermal collapse and in the bulk modulus, β, during pressure-induced collapse we show how zeolitic amorphization, although generally compressive, also involves decompression and how cavitation limits can be estimated. Moreover, by following small angle x-ray scattering after zeolite collapse we detect direct evidence for the coexistence of glass phases of different density. This finding is broadly similar to that of Deb and co-workers who in studying the amorphization of porous silicon reported the production of a high density amorphous phase on compression, with a low density amorphous phase being recovered at ambient pressure [10]. Both of these examples are consistent with the thermodynamic model of Ponyatovsky and Bartolov, where amorphization is related to the coexistence of two polymorphic states of different density but the same composition [15]. In particular, crystalline instability is associated with the unmixing of a supercooled liquid into a low density and a high density amorphous phase (LDA and HDA, respectively), the common boundary in $T-P$ space being the low temperature melting curve. In the second part of the paper we describe how

the dynamics of amorphization can be determined empirically from thermal- and pressure-induced processes by using different temperature and pressure ramp rates. These point to a universal relationship for the time course of zeolite collapse, comprising a dwell time followed by an Avrami-like nucleation process. Finally we show how the temperature dependence of the viscosity of the initial LDA phase in the thermodynamic model can be determined from the time to collapse, τ_A, and the collapse temperature, T_A. By comparing this with the structural relaxation time of a conventional glass extrapolated from the liquid state—HDA in the Ponyatovsky sense—we show how amorphization might be used to synthesize glasses with much smaller entropy than those prepared in the usual way by quenching from the melt.

2. Determining the instability limits between zeolites and the glasses amorphized from them

We have previously shown how temperature-induced amorphization of zeolites can be followed by x-ray diffraction (XRD) or wide angle x-ray scattering (WAXS) combined with x-ray absorption spectroscopy (XAS) [16] or with small angle x-ray scattering (SAXS) [17], using suitable multiple window muffle furnaces adapted to cover temperatures up to the softening point of vitreous aluminosilicates [18]. These combined x-ray techniques have employed multi-element solid state detectors for XAS [19], curved position detectors for XRD and quadrant detectors for SAXS, details of which are given elsewhere and are collated in [20]. For example figure 1 shows the recently commissioned SAXS/WAXS station MPW6.2 at the Synchrotron Radiation Source [20], and the collapse of the powder pattern zeolite A as it thermally amorphizes is illustrated in figure 2.

The decline in the crystalline fraction, x, measured during amorphization is shown in figure 3 alongside the fall in the coordination number of zinc obtained from XAS, measured in tandem. x is obtained from the changing area under the diffraction peaks and N_{Zn-O} from curve-fitting zinc EXAFS [16]. Figure 3 reveals how the loss of long range order in the zeolite is correlated with significant change in the local order around the charge compensating cation, zinc. This comparability, for example, reinforces the assumption we make here and elsewhere that the broadening of Debye–Scherrer lines during collapse is not a serious consideration in determining the crystalline fraction, x. Similar behaviour in XRD and XAS has been recorded for other cations used to balance the charge requirements of tetrahedral aluminium in zeolitic and amorphous aluminosilicate structures [11]. In figure 3, as elsewhere [13], the measured collapse sigmoid, x versus T, can be used to identify the point at which amorphization accelerates, T_1, and the point at which it decelerates, T_2. Midway we define the temperature of collapse, T_A, by $T(x = 0.5)$ and the time to collapse τ_A as the time to reach T_A from T_1, where r_T is the rate at which the temperature is increased. We use these systematics later to explore the dynamics of amorphization, when the rates of temperature increase or pressure increase are varied.

The basic results obtainable from SAXS/WAXS experiments are illustrated in figure 4(a), where the development of the SAXS invariant, Q_{SAXS}, during the amorphization of Na zeolite Y is plotted alongside the drop in the crystalline fraction, x. These are displayed both as a function of temperature and also of time. $Q_{SAXS} = \int_{q_{min}}^{q_{max}} I(q)q^2\,dq^n$, where $I(q)$ is the scattered intensity and $q = 4\pi \sin\theta/\lambda$ is the wavevector. This reflects the changing electron density contrast, $\Delta\rho_e$, between the zeolite, the LDA and the HDA phases present. Unlike the behaviour expected for a simple two-stage transformation for which $Q_{SAXS} \propto x(1 - x)$ and for which the scattered intensity would reach a maximum at $x = 0.5$, i.e. at T_A, the peak in Q_{SAXS} occurs when zeolite collapse is virtually over. In particular the electron density contrast, $\Delta\rho_e$, continues well beyond the temperature (and

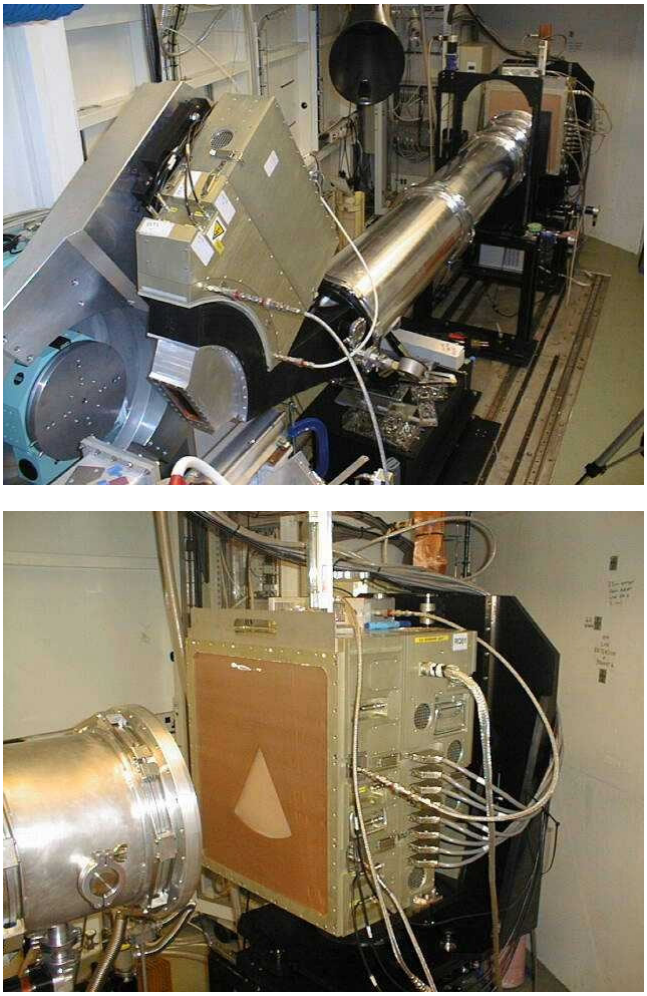

Figure 1. SAXS/WAXS set-up on MPW6.2 at the Synchrotron Radiation Source, showing the RAPID2 curved position sensitive detector and SAXS camera (top) and the quadrant RAPD SAXS detector (bottom) [20].

time) where the zeolite diffraction pattern has disappeared. This points to hereogeneity in the amorphized zeolite which can be most easily interpreted thermodynamically as resulting from the coexistence of LDA and HDA phases. Indeed a simple analysis of the Q_{SAXS} as a three phase system yields the fractions of zeolite, LDA and HDA phases at different stages during the amorphization process (see figure 4(b)) [22]. Using the fraction of zeolite, x, and assuming $\Delta\rho_{\mathrm{e}}(\text{zeolite–HDA}) = \Delta\rho_{\mathrm{e}}(\text{LDA–HDA})$, the different proportions of zeolite (squares), LDA (triangles) and HDA (inverted triangles) phases present at each temperature can be derived [22]. Although LDA and HDA phases coexist after collapse, it is the LDA phase that predominates initially, being gradually replaced by the HDA phase as amorphization concludes.

The glass transition temperatures corresponding to the high and low density phases are included in figure 4(a), where the high density glass transition (T_{g}HDA) is taken from literature values of feldspar liquids [23] averaged to the composition of the zeolite. The glass transition temperature of the low density phase (T_{g}LDA) is estimated from the temperature dependence

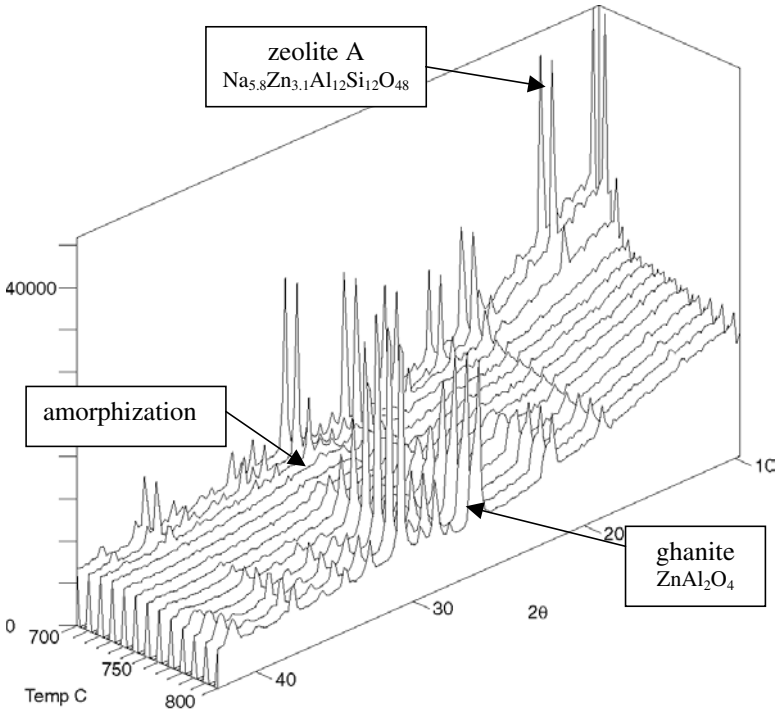

Figure 2. Following the thermally-induced amorphization of Zn exchanged Na zeolite A ($Na_{5.8}Zn_{3.1}Al_{12}Si_{12}O_{48}$) at 970 K with 10 s exposures [20]. At higher temperatures the aluminosilicate glass devitrifies with the nucleation of ghanite.

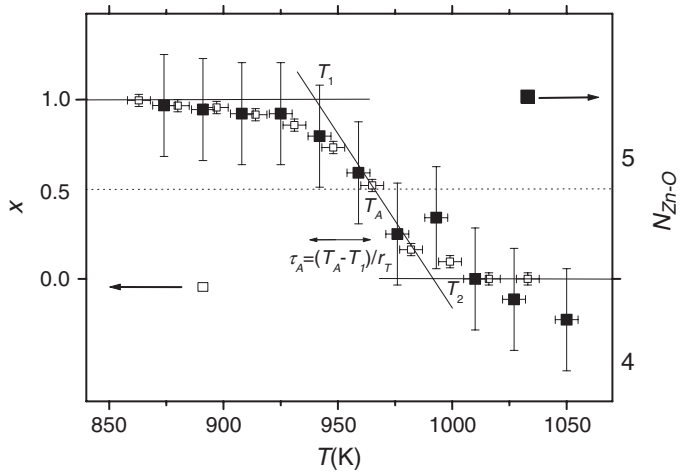

Figure 3. Collapse in the crystalline fraction of zeolite with temperature, x, for a zinc exchanged zeolite A, $Na_{5.8}Zn_{3.1}Al_{12}Si_{12}O_{48}$ (open points) compared with the coordination number of zinc, N_{Zn-O}, analysed from the K-edge EXAFS [16]. See the text for details.

of the collapse time, τ_A, and will be described later. It is clear that zeolite amorphization falls between these two glass transition temperatures. Accordingly the conversion of the low density amorphous phase to the high density amorphous phase implicit in figure 4(b) is

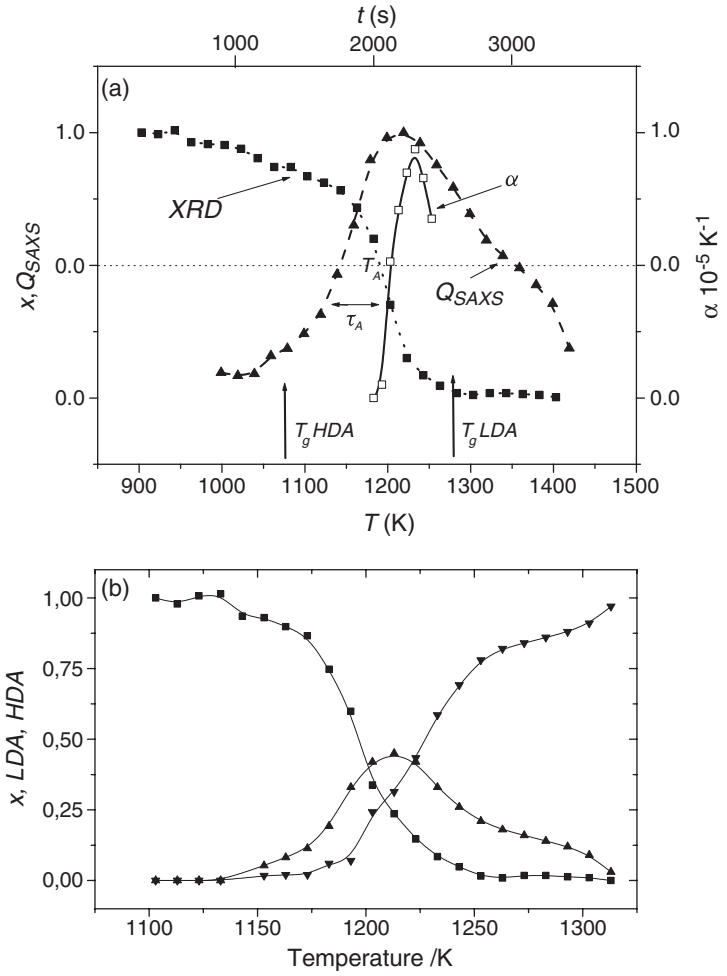

Figure 4. *In situ* SAXS/WAXS measurements following the amorphization of zeolite Y. (a) The crystalline fraction, x (filled squares), obtained from WAXS is contrasted with the SAXS invariant Q_{SAXS} (filled triangles) and the expansion coefficient α, referenced to the zeolite lattice parameter at ambient temperature. (b) Analysis of the SAXS invariant, Q_{SAXS} [22], to obtain the fractions of zeolite, LDA and HDA phases. x, T_{A} and τ_{A} are defined in figure 3. See the text for other details.

suggestive of a liquid–liquid phase transition, as simulated for instance in liquid silicon at lower viscosities [10] and already observed in liquid phosphorous [24]. However, unlike the density driven liquid–liquid phase transition model of Rapoport [25, 26], the transformation occurring in zeolitic amorphization does not appear to be reversible, presumably because the huge viscosities in operation prevent recovery of the topology of the low density LDA phase from the topology of the high density HDA phase. In all other respects both aluminosilicate phases appear tetrahedral, in which case they can only differ in the degree of chemical order which in turn is reflected in the mix of odd and even membered rings.

Figure 4(a) also includes anomalous behaviour in the thermal expansion coefficient, α, of the zeolite fraction. Measured from the lattice parameter, a, α $(=a^{-1}(\mathrm{d}a/\mathrm{d}T)_P)$ rises to a peak close to T_2. Zeolite amorphization is clearly accompanied by depressurization of the remaining zeolite, the zeolite providing a convenient calibrant of pressure. We have argued that

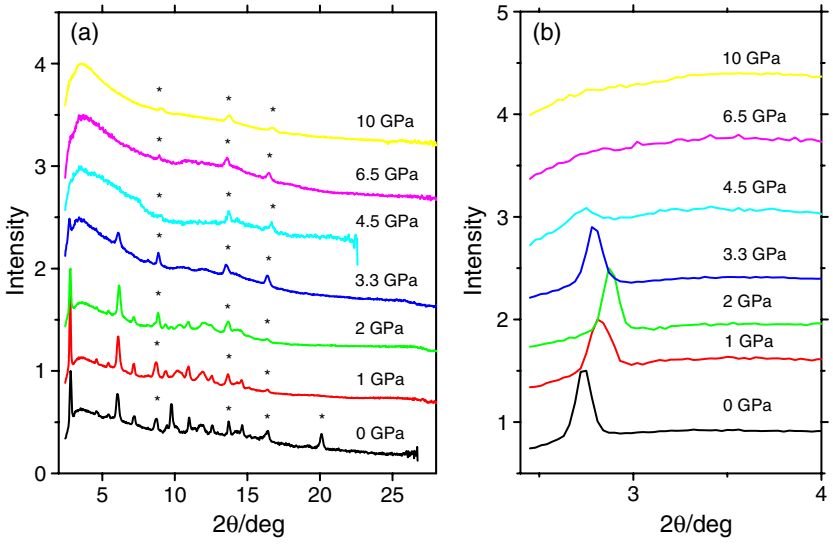

Figure 5. Pressure-induced amorphization of a Cd exchanged zeolite A ($Na_{8.75}Cd_{1.63}Al_{12}Si_{12}O_{48}$). The pressure was increased at 0.06 GPa min^{-1}. (a) Radially averaged image plate patterns taken from DAC measurements. (b) Changes in position of (100) peak with increasing pressure, showing the onset of decompression following the initial compression to 2 GPa.

the rise in α is due to amorphization nucleating stochastically within zeolite microcrystals [13] and from figure 4(b) this may well relate to the low density or LDA phase. If the LDA phase like the HDA phase is of lower density than the crystal, which is generally considered to be the case [15], and if amorphization nucleates within the crystalline bulk rather than at the surface, then local drops in specific volume, V, will occur which will generate internal tension randomly. Indeed such pockets of local pressure minima may further accelerate what appears to be a truly catastrophic process. If, as we will argue later, structural relaxation in the low density phase is reflected in the zeolite collapse time, τ_A, this will influence the recovery of ambient pressure within the residual crystalline component. As the zeolite fraction becomes overwhelmed by amorphization, the lattice parameter, a, is expected to pass through a maximum and return towards the pre-collapse value. From the ambient compressibility of zeolite A [13], β, the tensile stress within the zeolite reaches ~ -0.7 GPa. We refer to this point later as $-P(T_2)^*$ as it sets a boundary on cavitation that has been observed in SEM images of partially collapsed zeolites when these are thermally amorphized at very slow rates [13].

An example of pressure-induced amorphization for zeolite A is shown in figure 5. Measurements were made using a 0.3 mm focused 20.0 keV beam and a remotely pressurized diamond anvil cell (DAC). The pressure was recorded *in situ* from ruby fluorescence using a laser beam concentric with the x-rays. Full Debye–Scherrer patterns were detected with image plates and radially integrated. The pressure was increased in steps at a constant rate, collapse of the zeolitic structures occurring around 4 GPa. By choosing different pressure ramps, conditions can be found where the rate of collapse, τ_A^{-1}, is equivalent to that obtained for thermally-induced amorphization. This is illustrated in figure 6(a) for zeolite A. By comparison with figure 3, characteristic pressures can be identified for amorphization (P_A) and for the acceleration (P_1) and deceleration (P_2) of collapse, analogous with T_A, T_1 and T_2 in figure 3. These values can then be used (figure 6(b)) to map out regions of crystalline

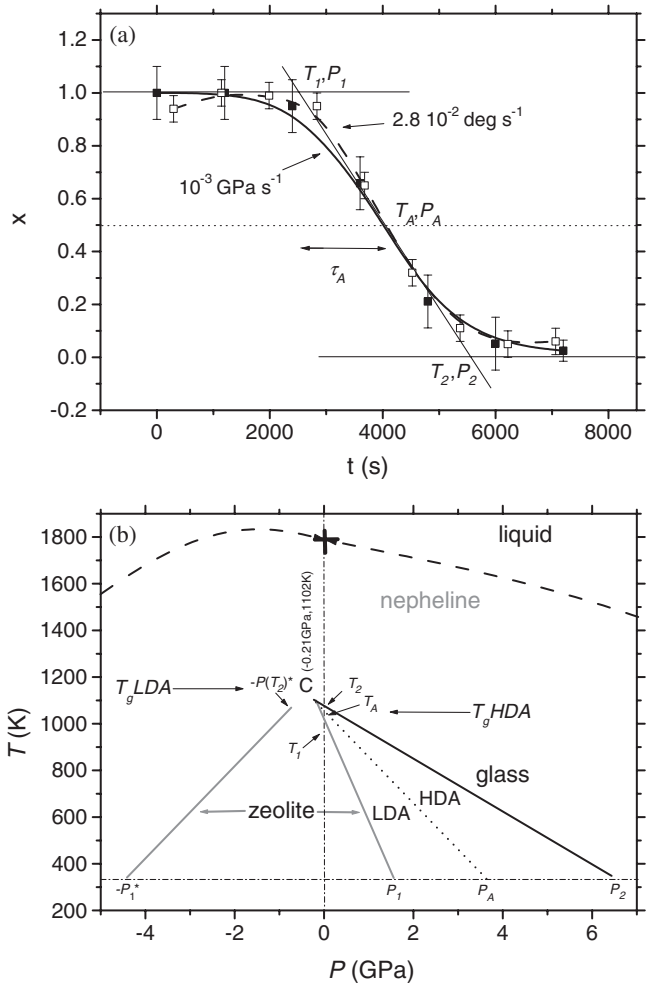

Figure 6. (a) Comparison between temperature- and pressure-induced amorphization of Cd exchanged zeolite A, x versus t, revealing similar values for the collapse time, τ_A, by either route. (b) $T-P$ phase diagram constructed from zeolite T_1, P_1 (grey) and glass T_2P_2 (black) boundaries and the amorphization curve, T_AP_A (dotted), separating LDA from HDA phases. The cross indicates the melting point of nephelene at ambient pressure (1800 K) and the dashed curve the melting curve inferred from the $T_1P_1P_2T_2$ instability zone.

and vitreous stability. The boundaries are shown simply as linear. HT–HP experiments are needed to establish their actual shape in $T-P$ space. At positive pressures zeolitic instability is clearly contained within $T_1P_1P_2T_2$, with the microporous crystal stable below T_1P_1 and the glass above T_2P_2. Together these define a critical point, C, at negative pressure where both glass and zeolite should coexist. Note how the glass transition temperatures of the low and high density phases, which were determined independently of experiments like figure 6(a), fall in the vicinity of the critical point, as expected in the LDA–HDA liquid mixing model of Rapoport [25, 26].

The triangular field for zeolite instability $T_1P_1P_2T_2$ can be modelled using the Ponyatovsky formalism [15]. The critical point, C, and the low temperature melting curve, T_AP_A, are used as the experimental input parameters in order to calculate the free energy for different mixtures

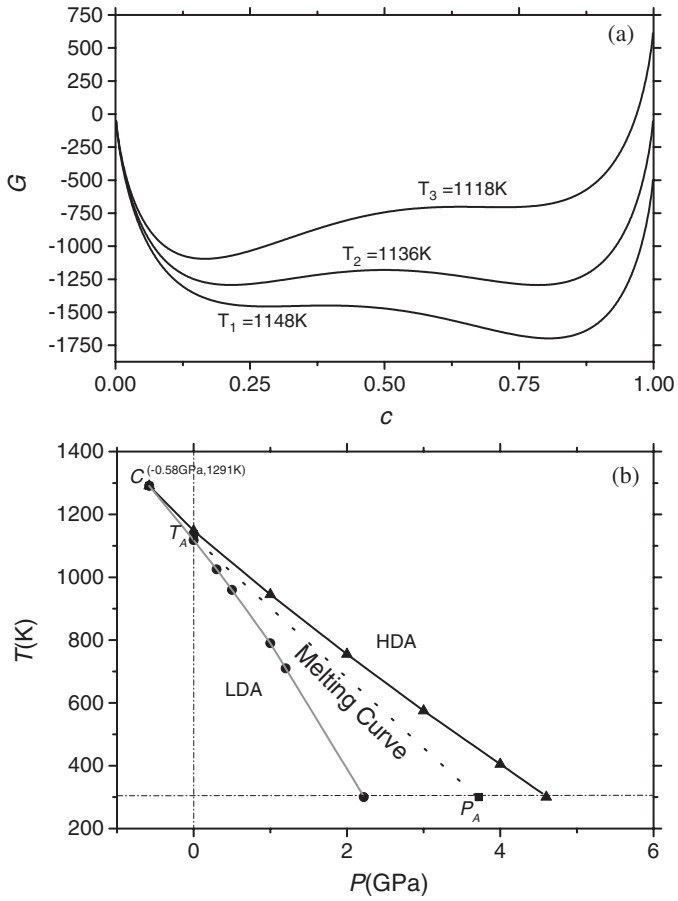

Figure 7. Linking the model of Ponyatovsky and Bartolov [15] with the results of zeolite amorphization. (a) Relationship between the free energy, G, of the low density amorphous (LDA) phase and the fraction of the high density amorphous (HDA) phase, c, at ambient pressure [22]. (b) Resulting $T-P$ phase diagram. The LDA and HDA boundaries correspond to the spinodal limits defined in (a) by $\mathrm{d}^2G/\mathrm{d}c^2$ and associated with the experimental boundaries, CP_1 and CP_2, like those illustrated in figure 6(b).

of LDA and HDA phases [22]. Figure 7(a) illustrates this for three different temperatures at ambient pressure. The spinodal points ($\partial^2 G/\partial c^2 = 0$) can be identified either side of the melting point. Extending this to other pressures provides the spinodal boundaries are shown in figure 7(b). The LDA limit lies close to the CP_1 line and the HDA limit to the CP_2 line that define the region of zeolite instability determined experimentally. We therefore associate the initial amorphous phase on collapse with the LDA phase and the final glass with the HDA phase [13].

During pressure-induced amorphization, it is clear from figure 5(b) that depressurization of the zeolite fraction occurs in an analogous way to temperature-induced amorphization (figure 4(a)). In this case the overall compressibility, $\beta = -V^{-1}(\mathrm{d}V/\mathrm{d}P)_T$, becomes zero close to P_1. For example, when the pressure is ramped for zeolite A the (100) peak returns to the starting ambient pressure value when the external pressure within the DAC has reached 4.5 GPa, signifying an internal pressure within the amorphous (LDA) phase of −4.5 GPa.

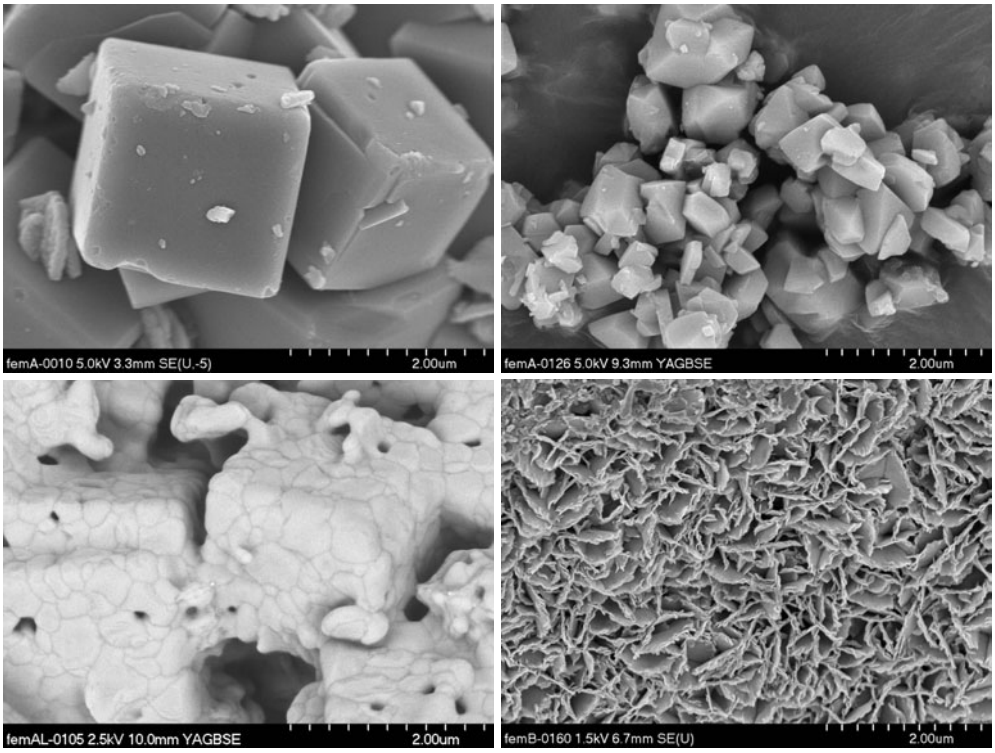

Figure 8. Cavitation effects observed during zeolite amorphization. Field emission scanning electron micrographs taken with a Hitachi s-470011 instrument. Pre-treated powders were coated with 5 nm Pt/Pd. (a) Na zeolite A: starting crystals (top) and partly thermally amorphized below T_gHDA (bottom). (b) Na zeolite Y: starting crystals (top) and partly pressure amorphized in a multi-anvil press (bottom).

We identify this as $-P_1^*$ in figure 6(b) and make the connection with $-P(T_2)^*$ to establish an empirical boundary for the stability of the LDA phase. At greater negative pressures the zeolite and or amorphous phase will cavitate. However, recent simulations of clathrate structures [9] indicate that low density crystalline structures should be preserved to at least −11 GPa. Liquids though are known to cavitate at lower negative pressures, and for liquid silicon, for example, this is simulated to occur around −4 GPa [9]. We have in fact observed cavitation phenomena during zeolite collapse as shown in the micrographs obtained *ex situ* in figure 8. In the case of temperature-induced amorphization ruptures open up within the crystal habits if the rate of temperature increase is slow and $T_A < T_g$HDA. For pressure-induced amorphization using a multi-anvil press at ambient temperature, crystals laminate in a striking fashion into a complex array of platelets of around 100 Å in thickness when the external pressure is released. In either case we presume that the failure occurs within the amorphous phase, either during zeolite collapse or as the LDA–HDA transformation takes place, as the increase in density in the amorphous phase is also expected to introduce local depressurization. Cavitation would appear to be a common occurrence in the collapse of microporous crystals when localized decompression is generated during the compressive amorphization process, provided that the viscosities are sufficiently high.

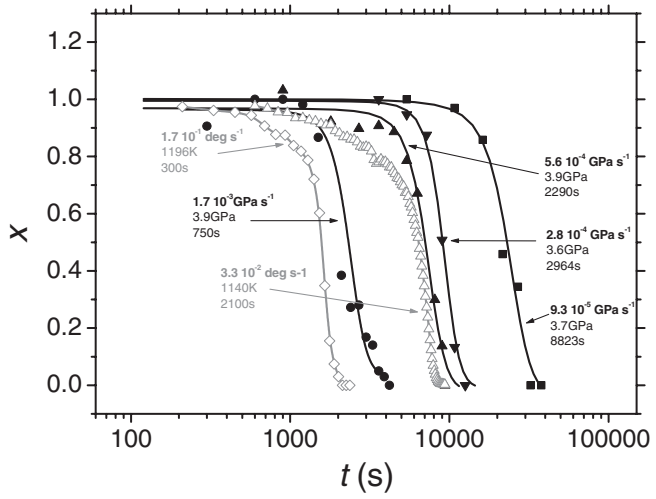

Figure 9. Equivalence of the amorphization of zeolites by temperature or pressure routes. Avrami-like sigmoids charting the collapse of Na zeolite Y as a function of temperature and pressure for different stress rates ranging from 2 to 10 °C min^{-1} (shown in grey) and from 0.0056 to 0.33 GPa min^{-1} (shown in black).

Taking the boundary defining zeolite instability in figure 6(b) ($T_1P_1P_2T_2$) together with the 1800 K melting point at ambient pressure of nephelene which has the same composition as zeolite A, these tentatively suggest that the melting curve might reach a maximum centred around 1–2 GPa. At positive pressures the slope is sketched negative as nepheline is expected to amorphize as do other feldspar minerals [6]. Finally we acknowledge that in figure 6(b) both the nepheline and zeolite fields experimentally occupy overlapping regions in the temperature–pressure diagram. The same is true of diamond silicon compared to silicon clathrates and porous silicon [9, 10], for example. Along with dehydrated zeolites, all of these microporous crystalline phases are intrinsically unstable at positive pressures and formally should occupy separate thermal equilibrium zones at negative pressure, as has recently been projected for silicon clathrates [9]. However, it is also true that microporous crystalline systems, synthesized as they are by low temperature *chemie douce* techniques, comprise rigid networks that share similarities with perfectly ordered glasses that potentially might be quenched via the glass transition from very high temperature superstrong liquids [27]. To date this has not proved to be a practical possibility

3. Dynamics of zeolitic amorphization and viscosity of LDA and HDA phases

The catastrophic nature of zeolite collapse is evident when different temperature or pressure ramps are employed. The faster the stress is applied, the shorter τ_A and higher the temperature, T_A, or pressure, P_A, that the microporous structure survives to. This is the phenomenon of sand piles and avalanches [28]. At the same time amorphization amounts to the same process irrespective of which route is taken, temperature or pressure. Figure 9 demonstrates this for zeolite Y heated or compressed at many different rates. The collapse sigmoids from XRD or WAXS are plotted as x versus t. Replotted as a function of reduced time, t/τ_A, they overlay to create a universal Avrami-like curve [13], with the approximate form $x = A\exp-(\frac{t-t_{\mathrm{dwell}}}{\tau_A})^n$. The exponent $n \sim 4$, which formally implies three-dimensional nucleation in a one step

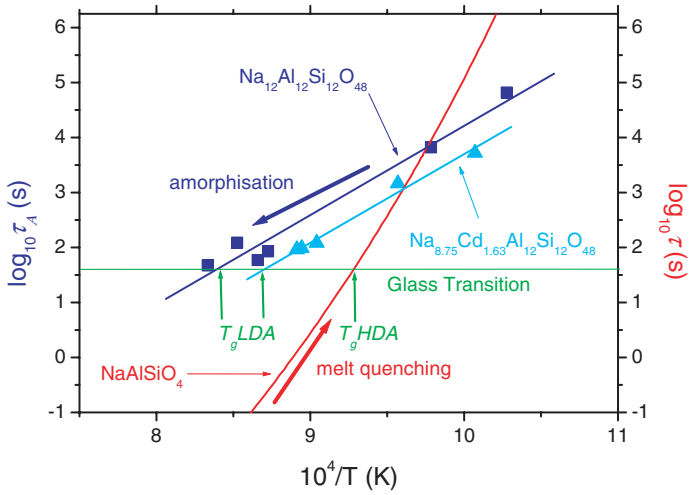

Figure 10. Zeolite amorphization kinetics, τ_A, for zeolite A compared to structural relaxation, τ, in liquid nepheline (taken from [23]). Collapse time data, $\log \tau_A$ versus $1/T$ plotted alongside viscosity data, $\log \tau$ versus $1/T$. The superstrong character evident in the Arrhenius temperature dependence of τ_A contrasts with the fragility of τ, the former being associated with and LDA phase and the latter with the conventional HDA phase. The bold arrows indicate how amorphization approaches the glass transition from low temperatures and the crystalline state whereas conventional glasses do so from high temperatures and the liquid state.

process. Furthermore, the dwell time, t_{dwell}, is equal to approximately $2\tau_A$ in almost all cases. This underscores the unstable character of the microporous crystalline structure at all positive pressures and for all temperatures in excess of ∼950 K when dehydration is complete.

The temperature dependences of the collapse time and temperature for different zeolites follow the Arrhenius Law, $\log \tau_A \propto 1/T_A$. This solid state rheology characteristic is illustrated for zeolite A in figure 10. Because zeolite amorphization appears to be closely associated with the formation of a low density or LDA phase, as identified in SAXS measurements (figures 4(a) and (b)), we have proposed that the dynamics of microporous collapse are determined by the structural response time of this liquid [13]. Over the wide range of amorphization temperatures and times explored with synchrotron techniques, the Arrhenius dependence indicates liquids with superstrong character. Fragility factors are half those of liquid silica, the classical strong glass-forming liquid and a small fraction of those of liquid nephelene, which we have equated with the HDA phase. Figure 10 therefore also includes the structural relaxation time for supercooled nepheline, obtained directly from viscosity measurements [23] using the classical relationship between viscosity, η, and structural relaxation time, τ, $\eta = G_\infty \tau$ mentioned earlier. The contrast is quite clear: nepheline liquid, along with many other aluminosilicate melts, conforms to the Tamann–Vogel–Fulcher law, $\tau = A \exp(\frac{B}{T-T_0})$, where T_0 is the so-called Kauzmann temperature where the configurational entropy of a melt-quenched glass is predicted to equate with that of the corresponding crystal [29]. For nepheline glass $T_0 = 623$ K [23], but achieving such a perfect glass is precluded by the requirement for infinitely slow cooling rates to depress T_g to this temperature.

There are two fascinating outcomes of the comparisons between the structural responses of the low and high density amorphous phases illustrated in figure 10. First we can read off values of both glass transition temperatures. The high-frequency shear modulus, G_∞, typically equals ∼25 GPa for feldspar liquids and as the glass transition is defined by $\eta = 10^{12}$ Pa s,

this is characterized for these glass-forming liquids by a structural relaxation time of ∼40 s, the faint line in figure 10. T_gHDA values like those of nepheline are of course already known directly from viscosity experiments; T_gLDA values not so. These are given by the vertical arrows in figure 10 for the sodium and cadmium exchanged zeolite compositions referred to earlier and are approximately 200 °C higher than the T_gHDA values of nepheline glass. Glass transition temperatures for the low density version of amorphized zeolite Y can be obtained similarly (figure 4(a)). As such the temperatures for low density glass transitions are indicative of very much stronger liquids than glass-forming liquids of conventional density and, as noted earlier (figures 4(a) and 6(b)), the T_gLDA and T_gHDA values straddle the temperature range of thermally-induced amorphization for normal heating rates and lie in the vicinity the critical point, C, in the Rapoport and Ponyatovsky thermodynamic models.

A second observation of the rheology of zeolite collapse concerns the large differences between the temperature dependences of the structural relaxation times of the low and high density liquids and the glasses they relate to. This means that, where for fast amorphization $\tau_A > \tau$ LDA liquids will quickly transform to the chemically disordered HDA phases, for slow amorphization $\tau_A < \tau$ and LDA phases might well be recovered, offering a route to synthesizing chemically ordered glasses. Such perfect glasses ideally share the same chemical order found in the crystalline state and may be harder and chemically more resistant than their conventional counterparts [30]. For pressure-induced amorphization the retention of low density phases may be even more likely, which could explain the remarkable petal-like morphology of the material released from a multi-anvil press (figure 7(b)). This has an overall density less than that of the starting zeolite and appears to have sprung open as the pressure of the press was removed. Basically, as figure 10 indicates, there should be a greater chance of acquiring chemical order in the amorphous state if the glass transition is approached from the crystalline state through amorphization than from the melt by cooling a suitably strong liquid, where configurational variety can only be annealed out over immense timescales [13]. The same principles for achieving chemically ordered or 'perfect glasses' should apply to amorphization from many other microporous crystalline materials.

Acknowledgments

Wim Bras, Odile Majerus, Gopinathan Sankar, Ken Walters and Rhodri Williams are thanked for useful discussions. Synchrotron radiation facilities were provided by the Synchrotron Radiation Source Daresbury Laboratory, where combined x-ray techniques were developed, and also by the Dutch-Belgium beam line (DUBBLE) at European Synchrotron Radiation Source in Grenoble.

References

[1] Mishima O, Calvert L D and Whalley E 1984 *Nature* **310** 393
[2] Muller G 1998 *Curr. Opin. Solid State Mater. Sci.* **3** 364
[3] De Carli P S and Jamieson J C 1959 *J. Chem. Phys.* **31** 1675
[4] Lin I J, Navid S and Grodzian D J M 1975 *Mineral. Sci. Eng.* **7** 313
[5] Skinner B and Fahey J J 1963 *J. Geophys. Res.* **68** 5595
[6] Richet P and Gillet P 1997 *Eur. J. Mineral.* **9** 907
[7] Liu L-G and Ringwood A E 1975 *Earth Planet. Sci. Lett.* **28** 209
[8] Sciortino F, Essmann U, Stanley H E, Hemmati M, Shao J, Wolf G H and Angell C A 1995 *Phys. Rev.* E **52** 6484
[9] Wilson M and McMillan P F 2003 *Phys. Rev. Lett.* **90** 135703
[10] Deb S K, Wilding M, Somayazulu M and McMillan P F 2001 *Nature* **414** 528

[11] Greaves G N 2000 *Phase Transitions and Self-Organisation in Electronic and Molecular Materials* ed J C Phillips and M F Thorpe (New York: Kluwer–Academic) (New York: Plenum)
[12] Greaves G N 2001 *Frontiers of High Pressure Research II: Application of High Pressure to Low Dimensional Electronic Materials* ed H D Hochheimer (New York: Kluwer–Academic) (New York: Plenum)
[13] Greaves G N, Meneau F, Sapelkin A, Colyer L M, ap Wynn I, Wade S and Sankar G 2003 *Nat. Mater.* **2** 622
[14] Zarzycki J 1991 *Glasses and the Vitreous State* (Cambridge: Cambridge University Press)
[15] Ponyatovsky E G and Bartolov O I 1992 *Mater. Sci. Rep.* **8** 147
[16] Colyer L M, Greaves G N, Carr S W and Fox K K 1997 *J. Phys. Chem.* B **101** 10105
[17] Bras W, Dolbnya I P, Detollenaere D, van Tol R, Malfois M, Greaves G N, Ryan A J and Heeley E 2003 *J. Appl. Crystallogr.* **36** 791
[18] Dent A J, Dobson B R, Greaves G N, Sankar G, Roberts M, Catlow C R A, Thomas J M and Rayment T A 1995 *Nucl. Instrum. Methods* B **97** 20
[19] Derbyshire G E, Dent A J, Dobson B R, Farrow R C, Felton A, Greaves G N, Morrell C and Wells M P 1992 *Rev. Sci. Instrum.* **63** 814
[20] Cernik R J, Barnes P, Bushnell-Wye G, Dent A J, Diakun G P, Flaherty J V, Greaves G N, Heely E L, Helsby W, Jacques S D, Kay J, Rayment T, Ryan A, Tang C C and Terrill N J 2004 *J. Synchrotron Radiat.* at press
[21] Greaves G N, Neneauu F and Sankar G 2003 *Nucl. Instrum. Methods* B **199** 98
[22] Meneau F 2004 Studies of the amorphisation of zeolites *PhD Thesis* University of Wales, Aberystwyth, UK
[23] Toplis M J, Dingwell D B, Hess K-U and Lenci T 1997 *Am. Mineral.* **82** 979
[24] Katayama Y, Mizutani T, Utsumi W, Shimomura O, Yamakata M and Funakoshi K-I 2000 *Nature* **403** 170
[25] Rapoport E 1967 *J. Chem. Phys.* **46** 2891
[26] Rapoport E 1968 *J. Chem. Phys.* **48** 1433
[27] Angell C A, Moynihan C T and Hemmati M 2000 *J. Non-Cryst. Solids* **274** 319
[28] Duran J 1999 *Sand Piles, Powders and Grains* (New York: Springer)
[29] Kauzmann W 1948 *Chem. Rev.* **43** 219
[30] Navrotsky A 2003 *Nat. Mater.* **2** 571